arXiv:2011.14738v1 [physics.optics] 30 Nov 2020

Significant Second-Harmonic Generation and Bulk Photovoltaic Effect in Trigonal Selenium and Tellurium Chains

Meijuan Cheng,† Xiaohong Shi,† Shunqing Wu,† and Zi-Zhong Zhu*,†

†*Department of Physics, Key Laboratory of Low Dimensional Condensed Matter Physics , Xiamen University, Xiamen 361005, China*

‡*Fujian Provincial Key Laboratory of Theoretical and Computational Chemistry, Xiamen 361005, China*

E-mail: zzhu@xmu.edu.cn

Abstract

One-dimensional selenium and tellurium crystalize in helical chainlike structures and thus exhibit fascinating properties. By performing first-principles calculations, we have researched the linear and nonlinear optical (NLO) properties of 1D Se and Te, and find that both systems exhibit pronounced NLO responses. In particular, 1D Se is found to possess large second-harmonic generation coefficient with the $\chi^{(2)}_{xyz}$ being up to 7 times larger than that of GaN, and even is several times larger than that of the bulk counterpart. On the other hand, 1D Te also produces significant NLO susceptibility $\chi^{(2)}_{xyz}$ which exceeds the bulk GaN by 5 times. Furthermore, 1D Te is shown to possess prominent linear electro-optic coefficient $r_{xxx}(0)$. Particularly, Te chain exhibits large shift current response and the maximum is more than the maximal photovoltaic responses obtained from $BaTiO_3$ by 2 times. Therefore, 1D Se and Te may find potential applications in solar energy conversion, electro-optical switches, and so on. Finally, much stronger NLO effects of 1D Se and Te are attributed to their one-dimensional structures with high anisotropy, strong covalent bonding and lone-pair electrons. These findings will contribute to the further study in experiments and search for excellent materials with large NLO effects.

INTRODUCTION

In the strong optical fields, materials with broken inversion symmetry will generate large nonlinear optical effects[1,2] such as second-harmonic generation (SHG), linear electro-optic (LEO) effect, bulk photovoltaic effect (BPVE). Second-harmonic generation(SHG), the best-known nonlinear optical (NLO) responses, have promising applications in probes of surfaces and interfaces, frequency doublers, and so on. Notably, it has been investigated extensively in bulk semiconductors[2–9] for nearly five decades beginning in the early 1960s. More recently, the family of NLO materials has also been extended to one-dimensional (see, e.g., refs 10-11 and references therein) and two-dimensional (see, e.g., refs 12-17 and references therein) systems, crucial for the development modern optical and electro-optical devices such as frequency conversions, electro-optic modulators, and switches.[2] As another second-order electric polarization effect, linear electro optic (LEO) effect refers to the linear refractive index variation (Δn) with the applied electric field strength (E), i.e., $\Delta n = n^3 r E/2$, here r is the LEO coefficient and n is the refraction index.[2] Therefore, the LEO effect could allow one to use an electrical signal to control the amplitude, phase, or direction of a light beam in the NLO materials, and leads to a widely used means for high-speed optical modulation and sensing devices (see, e.g., ref 18 and references therein). And more notably, the bulk photovoltaic effect (BPVE), a third nonlinear optical response, has become a vibrant research topic in recent years. Unlike traditional photovoltaics, the BPVE can be obtained in single crystal with the broken inversion symmetry, which is extremely ponderable for solar energy collection and conversion.

The crystal structures of trigonal selenium and tellurium consist of the helical chains arranged in a hexagonal array, with their axes parallel to the c axis. Along the chain, every atom is covalently bonded to two neighboring atoms, and interacts with four second nearest-neighbor atoms of the adjacent chains by relatively weaker interaction, or more precisely, covalent-like quasi-bonds (CLQB),[19] thus indicating that they may allow to be exfoliated as the individual atomic chains. Excitingly, Li *et al.* reported the fabrication process of single

Se chains and the experimental study of the geometry, phase stability, electronic properties, and so on.[20] More recently, Churchill *et al.* demonstrated the potential for fabrication of isolated tellurium atom chains by mechanical exfoliation in experiment.[21] The experimental breakthrough triggered a growing renewed interest in 1D selenium and tellurium.[22–28] In particular, Se and Te chains maintain the interesting nature of Se and Te bulks, i.e., broken spatial inversion symmetry, and thus make the 1D systems possess fascinating properties such as nonlinear optical responses, piezoelectric and ferroelectric properties.

As elemental semiconductor materials, 1D selenium and tellurium chains has been investigated extensively in the structural, electronic, and linear optical properties.[22–28] However, there is no systematic study on second-order nonlinear optical responses of these helical atomic chains to date. It is well known that low dimensional semiconductors could possess attractive properties not seen in their bulk counterparts, for example, spin-valley coupling,[29] and further have attracted widespread attention in recent years. Indeed, having band gap in the visible spectrum (1.6-3.1 eV), the Se and Te chains could be expected to show significant BPVE response and then equip potential applications in solar energy harvesting.

In this work, we perform first principles calculations of the linear dielectric functions, the second-order NLO susceptibility, linear electro-optic effect and the bulk photovoltaic effect for 1D selenium and tellurium. Our main purpose is to find out the magnitude and characteristics of NLO effects in both systems and thus predict whether they have any potential applications in the domain of nonlinear optics such as electro-optic modulator, frequency multiplier, optical switching, and sum-frequency generation. Accordingly, to motivate the potential applications and experimental developments of Se and Te chains in the near future, we systematacially investigate the NLO properties of these chain structures.

COMPUTATIONAL DETAIL

In this paper, we study the electronic property, optical dielectric function, SHG and LEO coefficients over the entire optical frequency range, as well as the shift current (SHC) response. The crystal structure of 1D selenium or tellurium is schematically displayed in Fig. 1. It consists of three atoms in the unit cell situating at positions $(u, 0, 0)$, $(0, u, 1/3)$ and $(-u, -u, 2/3)$. The valence electron configurations of 1D selenium and tellurium are $4s^2 4p^4$ and $5s^2 5p^4$, respectively. That is one third of the p bands are empty and thus every atom is covalently bonded to two neighboring atoms along helical chain. For selenium and tellurium bulks, coordination number of atoms is 6, whereas that of single helical chain reduces to 2. Consequently, intrachain distances in single helical chain are shorter than that of bulks due to the lower coordination number of atoms (see Table 1). The 1D structures are modeled by using the slab-superlattice approach with a 20 Å thickness of the vacuum region along the a and b-direction, ensuring negligible interaction between the periodic images. The effective unit cell volumes of 1D systems are expressed as $V_{eff} = (V \cdot a \cdot b)/(20\text{Å} \cdot 20\text{Å})$, here a and b are corresponding lattice constants of bulks, rather than the arbitrary volume of the supercells V.

Table 1: Calculated lattice constant c, the distances of intrachain r, effective unit cell volume V_{eff}, calculated band gap with GGA (E_g^{GGA}) and the HSE calculations with the SOC ($E_g^{HSE-SOC}$) as well as scissors operator ($\Delta E_g = E_g^{HSE-SOC} - E_g^{GGA}$) for selenium and tellurium chains.

	c (Å)	r (Å)	V_{eff} (Å^3)	E_g^{GGA} (eV)	$E_g^{HSE-SOC}$ (eV)	ΔE_g (eV)
Se bulk	4.954[a]	2.373[a]	81.78[a]	1.002[a]	1.735[a]	0.733[a]
Se chain	4.956 (4.949)[c]	2.363	81.82	1.992(2.043)[c]	2.859	0.867
Te bulk	5.926[a]	2.833[a]	101.68[a]	0.113[a]	0.322[a]	0.209[a]
Te chain	5.690(5.69)[b](5.651)[c]	2.747 (2.74)[b]	97.63	1.666(1.750)[c]	2.194	0.528

[a] Reference 8.
[b] Reference 24.
[c] Reference 27.

Our ab initio calculations are performed using the accurate projector augmented wave (PAW) method,[30] as implemented in the Vienna ab initio simulation package,[31,32] They are

based on the density-functional theory with the generalized gradient approximation (GGA) of Perdew, Burke, and Ernzerhof.[33] An adequately large plane-wave cutoff (E_{cut}) of 450 eV is adopted throughout and the total energy convergence criterion for the self-consistent electronic structure calculations is 10^{-6} eV. The atomic positions and lattice constants are fully relaxed until the forces acting on all the atoms are less than 0.001 eV/Å. K-point meshes of 1×1×40 for Se and Te single helical chains are used for the self-consistent charge density calculations. Further calculations using different k-point meshes indicate that the above k-point meshes yields the well-converged charge density.

In our work, the linear optical dielectric function, second-harmonic generation (SHG), linear electro-optic (LEO) effect and the shift current (SHC) response are calculated based on the linear response formalism with the independent-particle approximation, as described previously.[10,34] The imaginary part of the dielectric function $\varepsilon(\omega)$ is given by the Fermi golden rule due to direct interband transitions. The real part of the dielectric function is obtained from the calculated $\varepsilon''(\omega)$ by the Kramer-Kronig transformation. As previously reported, the imaginary part of the second-order optical susceptibility due to direct interband transitions is given by[10,11]

$$\chi''^{(2)}_{abc}(-2\omega,\omega,\omega) = \chi''^{(2)}_{abc,VE}(-2\omega,\omega,\omega) + \chi''^{(2)}_{abc,VH}(-2\omega,\omega,\omega), \tag{1}$$

where the contributions are derived from the so-called virtual-electron process $\chi''^{(2)}_{abc,VE}$ and the virtual-hole process $\chi''^{(2)}_{abc,VH}$.[10,11] Then the real part of the second-order optical susceptibility $\chi'^{(2)}_{abc}$ is obtained from the calculated imaginary part $\chi''^{(2)}_{abc}$ by the Kramer-Kronig transformation. The linear electro-optic $r_{abc}(\omega)$ is related to the second-order optical susceptibility $\chi^{(2)}_{abc}(-\omega,\omega,0)$.[5] In the zero frequency limit, $r_{abc}(0)$ is expressed as

$$r_{abc}(0) = -\frac{2}{\varepsilon_a(0)\varepsilon_b(0)} \lim_{\omega\to 0} \chi^{(2)}_{abc}(-2\omega,\omega,\omega). \tag{2}$$

For the photon energy ω well below the band gap, $\chi^{(2)}_{abc}(-2\omega,\omega,\omega)$ and $n(\omega)$ are nearly con-

stant and then the LEO coefficient $r_{abc}(\omega) \approx r_{abc}(0)$.[12] Furthermore, we calculate the major origins of the bulk photovoltaic effect, i.e., the shift current, by the following equation,[35]

$$J_a(\omega) = \sum_{bc} \sigma_{abc}(\omega) E_b(\omega) E_c(\omega). \tag{3}$$

Where the third-rank tensor $\sigma_{abc}(\omega)$ could be given by using the expression from ref 32.

In order to obtain accurate optical properties, several different k-point grids are calculated for selenium and tellurium chains until the calculated optical properties converge to a few percent. In conclusion, we use a denser enough k-point meshes of 2×2×120 for 1D Se and Te chains. Test calculations indicate that using 30 bands per atom included in the optical calculations is sufficiently accurate for $\varepsilon'(\omega)$ and $\chi'^{(2)}_{abc}$ obtained by the Kramer-Kronig transformation. Furthermore, the calculated optical spectra are broadened by using a Gaussian function with $\Gamma = 0.2$ eV.

As mentioned above, our calculated linear and nonlinear optical properties are based on the independent-particle approximation (IPA), i.e., the quasi-particle self-energy corrections and excitonic effects were neglected. However, low dimensional materials possess quantum confinement and thus many-body effects play a remarkable role on the linear optical properties of low dimensional systems such as MoS_2 ML, SiC sheet.[36,37] It is widely known that precise first-principles calculations considering the excitonic effect such as GW approximation combined with the Bethe-Salpeter equation (BSE) could produce sufficiently accurate optical spectra compared to experimental measurements.[37] Nevertheless, these approaches are performed on the basis of several thousand k-points and tens of bands and then are usually extremely demanding computationally. Worse still, the expression for nonlinear susceptibility is much more complicated than that of the linear optic, resulting in failure to perform the full first-principles calculations with many-body effects included. As a result, much simpler approaches such as the real-time propagation,[38] scissors correction (SCI)[12] and semiempirical tight-binding-based model potential[39] were used to calculate nonlinear

optical property. Similarly, we take the self-energy corrections into account by the so-called scissors correction (SC) to reduce the errors of calculated linear dielectric function and NLO coefficients caused by neglected many-body effects. Indeed, such SC calculations have been testified to generate the NLO susceptibility at zero frequency for low-dimensional materials such as graphene-like BN sheets[12] that agree well with the experimental ones.

RESULTS AND DISCUSSION

Band Structures of Se and Te Chains

The calculated band structures of selenium and tellurium chains are extremely similar due to the same crystalline structures, as displayed in Figure 2. Both systems are indirect band-gap semiconductors with the conduction band minimum (CBM) being at the A point, whereas the valence band maximum (VBM) is located somewhere slightly closed to A along the Γ-A symmetry line. The valence bands of two materials could be divided into three groups, arising from s bonding, p bonding, and p lone pair states, respectively, and the three lowest conduction bands are corresponding to the p antibonding states. Compared to bulk systems, less electrons transferred from lone pair states to antibonding states since interchain interaction is not reside in one-dimensional chain structures. This explains why the calculated band gap of 1D Se and Te is much larger than that of bulk counterparts, especially for tellurium chain. Obviously, the band gap we calculated with GGA agrees rather well with previous results[27] (see Table 1).

As mentioned previously,[8] the band gaps calculated by the GGA are generally underestimated. Thus, to obtain accurate optical properties that are on the basis of precise band structure, we also calculate the band structures using the hybrid Heyd-Scuseria-Ernzerhof (HSE) functional[40] with the SOC included, as shown in Fig. 2. Indeed, in our precious report,[8] the comparison of HSE-SOC band gaps and experimental values for bulks proves that the HSE calculations with the SOC is sufficiently accurate in describing band gap. There-

fore, all the optical properties in 1D materials are calculated from the GGA band structures based on the scissors correction (SCI).[12] The scissors correction energy, i.e., the differences between the HSE-SOC and GGA band gaps, and HSE-SOC band gaps are listed in Table 1.

Linear Optical Property of Se and Te Chains

The calculated imaginary and real part of dielectric function for one-dimensional selenium and tellurium are displayed in Fig. 3. Similar to bulk systems, 1D counterparts are uniaxial crystalline structures with strongly covalent bonded helical chains oriented along the c axis and then their optical properties are strongly dependent on light polarization direction. As a result, the constituent elements of dielectric function are two significantly different components, namely light polarization parallel ($E \parallel c$) and perpendicular ($E \parallel a$) to the c axis. Apparently, the spectral feature of dielectric function for selenium chain is extremely similar to that of tellurium due to the same crystalline structures. Hence, in what follows, we will take that of 1D Se as an example to perform a detailed analysis [see Fig. 3(a) and (b)]. As expected, stronger anisotropy in the spectra of dielectric function can be observed. This could be explained by the fact that the two systems possess a much stronger structural anisotropy than bulks. Figure 3(a) shows that the spectra of the imaginary part of the dielectric function for Se chain could be conveniently divided into two regions. Due to different optical selection rules, in the low-energy region (about 2.5-5.5 eV), there is prominent optical absorption for $E \parallel c$, whereas, the greatly weak absorption is observed in the range of energy for $E \parallel a$. Furthermore, our calculations predict two rather remarkable peaks in the imaginary part of the dielectric function for $E \parallel c$ (direction of chains) within the energy region, i.e., a much larger peak located at $\sim$3.9 eV and a slightly small one in the vicinity of 3.1 eV. In the energy range from 5.5 to 14.0 eV, one-dimensional selenium exhibits a pronounced peak at $\sim$7.5 eV and a relatively small peak near 6.8 eV in the spectrum of $\varepsilon''(\omega)$ for $E \parallel c$. However, the spectrum of $E \parallel a$ exhibits some steadily oscillatory bulges and a relatively weak peak centered at $\sim$8.3 eV. In particular, a deep minimum occurs at $\sim$5.5 eV originating from

the fact that transitions from the upper valence triplet to the lower conduction triplet are already exhausted. Beyond that, the increase in the spectral amplitude within the energy range between 5.5 eV and 14.0 eV is due to the transitions from the lower valence triplet to the lower conduction triplet and also from the upper valence triplet to the upper conduction triplet.

Second-Harmonic Generation and Linear Electro-Optic Coefficient of Se and Te Chains

Similarly to bulk materials, one-dimensional selenium and tellurium also possess five nonzero nonlinear susceptibility and only two elements are independent, i.e., $\chi^{(2)}_{xxx} = -\chi^{(2)}_{xyy} = -\chi^{(2)}_{yxy}$, $\chi^{(2)}_{xyz} = -\chi^{(2)}_{yzx}$. Notably, based on the scissors correction, the peak positions are blue-shifted by about the energy of the scissors correction (ΔE_g) and the magnitude of the SH susceptibility gets reduced (see Table 2), while the line shapes of SHG spectra are hardly changed. As a result, only the results obtained with scissors correction are displayed in this paper. The static values of the dielectric constant, LEO coefficient and second-order NLO susceptibility in the 1D selenium and tellurium are listed in Table 2. Compared with bulk Se and Te,[8] the static SHG coefficients for Se and Te chains decrease which, however, are comparable to that of GaN in both zinc-blende and wurtzite structures.[6,7] In addition, Te chain possesses large LEO coefficient $r_{xxx}(0)$ (∼1.5 pm/V), exceeding 2 times larger than that of bulk GaN polytypes.[6,7]

Table 2: Static dielectric constants ($\varepsilon_x = \varepsilon_y$ and ε_z), second-order susceptibility $\chi^{(2)}_{xxx}(0)$ (pm/V) and $\chi^{(2)}_{xyz}(0)$ (pm/V) as well as LEO coefficient $r_{xxx}(0)$ (pm/V) and $r_{xyz}(0)$ (pm/V) of selenium and tellurium chains calculated without (GGA) and with (SC) scissors correction.

		ε_x	ε_z	$\chi^{(2)}_{xxx}(0)$	$\chi^{(2)}_{xyz}(0)$	$r_{xxx}(0)$	$r_{xyz}(0)$
Se chain	GGA	5.1	12.7	19	7	-1.48	-0.50
	SC	4.6	10.3	9	2	-0.87	-0.16
Te chain	GGA	6.8	16.7	54	49	-2.33	-2.10
	SC	6.3	14.2	29	23	-1.46	-1.15

The calculated real and imaginary parts as well as the absolutes values of the second-order susceptibility are presented in Figs. 4 and 5 for selenium and tellurium chains, respectively. Apparently, the real and imaginary parts of second-order NLO susceptibility for both systems show an oscillatory behavior. Indeed, for Se chain, the spectrum of absolute value of the SH generation coefficients oscillates rapidly and dominating values are distribute in the photon energy range of 1.0-7.0 eV [see Figs. 4(b) and 4(e)]. Furthermore, the absolute value of $\chi^{(2)}_{xyz}$ reaches the maximum ∼1502 pm/V at ∼3.0 eV which, notably, is nearly 7 times larger than that of GaN,[6,7] a widely used NLO semiconductor, and even is several times larger than that of bulk counterpart. This indicates that one-dimensional selenium would be excellent nonlinear optical materials and have potential applications in the field of nonlinear optics such as second-harmonic generation, frequency conversion, optical switching, optical modulation, and so on. Unlike Se chain, the oscillatory spectra of the second-order NLO susceptibility in 1D Te are none the less significant over the entire optical frequency range and the maximal NLO susceptibilities tensor $|\chi^{(2)}_{xyz}|$ is as high as 1219 pm/V at 2.34 eV, which exceeds 5 times larger than that of GaN.[6,7] Significantly, for both materials, the real part, imaginary part, and absolute value of $\chi^{(2)}_{xyz}$ are larger than $\chi^{(2)}_{xxx}$, which is contrary to bulk counterparts. The phenomenon could be explained by the fact that the two systems are one-dimensional spiral chains along the c axis and have a high degree of anisotropy.

The SHG involves not only single-photon (ω) resonance but also double-photon (2ω) resonance. Therefore, to further analyze the NLO responses and understand the prominent features in the spectra, we also exhibit the dielectric functions $\varepsilon''(\omega)$ and $\varepsilon''(\omega/2)$ together in Figs. 4 and 5 for 1D selenium and tellurium, respectively. Because of similar features, in the following section, we only take the second-order susceptibility element $\chi^{(2)}_{xyz}$ of 1D Te as an example to perform a brief analysis. Figs. 5(e) and 5(f) show that the threshold of the $\chi^{(2)}(-2\omega,\omega,\omega)$ spectra is corresponding to the absorption edge of $\varepsilon''(\omega/2)$, i.e., ∼ 1.0 eV (∼ $\frac{1}{2}E_g$), while the absorption edge of $\varepsilon''(\omega)$ is close to the band gap value E_g (∼2.0 eV). Therefore, the second-order NLO susceptibility spectra can be divided into two parts.

The first part from ∼1.0 to ∼2.0 eV is formed by double-photon resonances. The second part (above ∼2.0 eV) is associated single-photon resonances with contribution from double-photon resonances [see Fig. 5(f)]. Apparently, these two types of resonances cause the SHG spectra to violently oscillate and finally decrease gradually in the higher energy region.

Bulk Photovoltaic Effect of Se and Te Chains

The bulk photovoltaic effect (BPVE) is of the utmost importance to solar energy harvesting, which can be observed in single-phase homogeneous materials without inversion symmetry. Moreover, the shift-current (SHC) is dominating mechanism of the bulk photovoltaic effect (BPVE). Therefore, in our work, we have calculated the SHC coefficients for one-dimensional selenium and tellurium. Due to specific symmetry class, the calculated SHC coefficients possess same nonzero elements with that of second-order NLO susceptibility, i.e., σ_{xxx}=−σ_{xyy}=−σ_{yxy}, σ_{xyz}=−σ_{yzx}. Similar to second-order NLO susceptibility, the spectra of the shift-current in both systems exhibit significant oscillatory behavior and distribute in a broad range of energy, as displayed in Fig. 6. Furthermore, our calculations for two helical structures also reveal that the maximal value of the shift current responses σ_{xxx} is larger than that of σ_{xyz}, and is opposite in sign. Obviously, the threshold of shift current spectra and the absorption edge of the imaginary part of the dielectric function are approximately equal, in spite of small and flat. The maximal element σ_{xxx} in 1D Se exhibits a prominent peak near 10.1 eV, which is larger than the maximum response observed for $BaTiO_3$,[41] an archetypical single-crystal with the bulk photovoltaic effect. Interestingly, our calculations predict that Te chain exhibits more pronounced shift current response and the maximum in SHC coefficient σ_{xxx} is more than the maximal photovoltaic responses obtained from $BaTiO_3$ by 2 times.[41] Overall, our results indicate that one-dimensional selenium and tellurium, especially for tellurium, are outstanding broadband photovoltaic materials and possess potential application prospects in solar energy conversion. Therefore, one could expect our calculations would boost further research on the experiments and potential applications. Furthermore,

such remarkable SHC response can be attributed to strong covalent bond in 1D Se and Te which, in what follows, will be explained in detail.

It is widely known that the smaller the band gap is, the larger the magnitude of the imaginary part of the dielectric function, and NLO responses would be, as explained in our previous work,[8] only due to the energy differences between the initial and final states of optical excitations in the denominators. Particularly, the magnitude of the imaginary part of the second-order NLO susceptibility, especially in the low frequency region, would be approximately proportional to the inverse of the fourth power of the band gap. However, compared to common semiconductors with semblable band gaps,[13,42–49] one-dimensional selenium and tellurium exhibit much larger second-order NLO responses. To further investigate the origins of the enhanced NLO effects of one-dimensional systems, we calculate the deformation charge density, as depicted in Fig. 7. Clearly, considerable electrons accumulate in the neighborhood of the Se-Se (Te-Te) bond center by exhausting the electrons around the atoms in the direction of the bond, and then lead to the strongly directional covalent bonds. Strong covalency is beneficial to large spatial overlap between the wave functions of initial and final states resulting in large optical matrix elements, and thus give rise to large SHG values. Furthermore, Fig. 7 also displays charge accumulate around each atom in the direction perpendicular to the chain, indicating the presence of lone-pair electrons. Notably, lone-pair electrons are to the benefit of the generation of induced dipole oscillations by the optical electric fields, thus resulting in enhanced NLO responses.[50,51] There is, in addition, one further point is high anisotropy for one-dimensional materials, which would lead to large joint DOS, would bring large $\chi^{(2)}$ into being.[52,53] As a result, much larger linear and nonlinear optical responses in one-dimensional selenium and tellurium attribute to strong covalency, lone-pair electrons, high anisotropy. Similar to band gap, the volume, another crucial quantity in optical effects, is also reflected in the denominators of the equations for imaginary part of the dielectric function and second-order NLO susceptibility, thus suggesting that the large volume is to the disadvantage of pronounced optical responses. Being compared with bulk

counterpart, 1D Se chain possesses higher anisotropy and comparable volume, in spite of increased band gap. This explains that selenium chain has larger SHG coefficients than that of selenium bulk. Conversely, even though 1D Te exhibits higher anisotropy and comparable volume, the greatly enhanced band gap results in much smaller NLO values. Therefore, in general, to search for excellent NLO materials, one could focus on those semiconductors with smallest possible band gaps which are larger than the optical frequencies required by specific NLO applications, strong covalency, lone-pair electrons, high anisotropy and small volume.

CONCLUTIONS

Summarizing, we have performed a systematic first-principles calculations of the linear and nonlinear optical properties of one-dimensional selenium and tellurium based on DFT within the GGA plus scissors correction. Compared to the common semiconductors with similar band gaps, 1D Se and Te chains exhibit enhanced SHG, LEO as well as SHC responses. Also, due to their structural anisotropy, the linear and nonlinear optical effects manifest stronger anisotropy than the corresponding bulk systems. Especially, one-dimensional selenium exhibits remarkable SH generation coefficient with the $\chi^{(2)}_{xyz}$ being nearly 7 times larger than that of GaN, a widely used NLO semiconductor. On the other hand, 1D Te is found to possess large second-order NLO susceptibilities $\chi^{(2)}_{xyz}$ being as large as 1219 pm/V, which is more than five times larger than that of GaN. Furthermore, Te chain exhibits prominent LEO coefficient which exceeds the bulk GaN polytypes by 2 times. It's worth noting that 1D Te is shown to have large shift current (SHC) response and the maximum is more than the maximal photovoltaic responses obtained from $BaTiO_3$ by 2 times. The maximal shift current element in 1D Se is also larger than $BaTiO_3$, an archetypical single-crystal with the bulk photovoltaic effect. Thus, 1D Se and Te may have application potentials in solar energy conversion, second-order nonlinear optical devices and linear electro-optic modulators, and so on. The prominent structures in the $\chi^{(2)}$ spectra of 1D Se and Te have been

successfully associated with single-photon and double-photon resonances. Finally, enhanced NLO effects in 1D selenium and tellurium compared to the general semiconductors with similar band gaps ascribe to their one-dimensional structures with lone-pair electrons, high anisotropy, strong covalency. This also indicates a strategy to search for excellent NLO materials with a specified band gap, i.e., starting with chainlike semiconductors with strong covalency and/or lone-pair electrons, high anisotropy. We expect that our work will stimulate further experiments and practical application on the SHG, LEO and SHC responses in these lower-dimensional materials.

Acknowledgement

M. J. Cheng thanks G.-Y. Guo of Department of Physics and Center for Theoretical Physics, National Taiwan University for his hospitality during her three months visit there. The work is supported by the National Key R&D Program of China (Grant No. 2016YFA0202601), and the National Natural Science Foundation of China (No. 11574257).

References

(1) Shen, Y. R. *The Principle of Nonlinear Optics* (John Wiley and Sons Inc., New Jersey, 2003).

(2) Boyd, R. W. *Nonlinear Optics* (Elsevier Science, Amsterdam,2003).

(3) Chang, R. K.; Ducuing, J.; Bloembergen, N. Dispersion of the Optical Nonlinearity in Semiconductors. *Phys. Rev. Lett.* **1965**, *15*, 415-418.

(4) Zhong, H.; Levine, Z. H.; Allan, D. C.; Wilkins, J. W. Band-theoretical calculation of the optical activity tensor of α-quartz and trigonal Se. *Phys. Rev. B* **1993**, *48*, 1384-1403.

(5) Hughes, J. L. P.; Sipe, J. E. Calculation of second-order optical response in semiconductors. *Phys. Rev. B* **1996**, *53*, 10751-10763.

(6) Gavrilenko, V. I.; Wu, R. Q. Linear and nonlinear optical properties of group-III nitrides. *Phys. Rev. B* **2000**, *61*, 2632-2642.

(7) Cai, D. J.; Guo, G.-Y. Tuning linear and nonlinear optical properties of wurtzite GaN by *c*-axial stress. *J. Phys. D: Appl. Phys.* **2009**, *42*, 185107.

(8) Cheng, M. J.; Wu, S. Q.; Zhu, Z.-Z.; Guo, G.-Y. Large second-harmonic generation and linear electro-optic effect in trigonal selenium and tellurium. *Phys. Rev. B* **2019**, *100*, 035202.

(9) Ni, B. L.; Sun, W. M.; Kang, J.; Zhang, Y. F. Understanding the Linear and Second-Order Nonlinear Optical Properties of UiO-66-Derived Metal-Organic Frameworks: A Comprehensive DFT Study. *J. Phys. Chem. C* **2020**, *124*, 11595-11608.

(10) Guo, G. Y.; Chu, K. C.; Wang, D.-S.; Duan, C.-G. Linear and nonlinear optical properties of carbon nanotubes from first-principles calculations. *Phys. Rev. B* **2004**, *69*, 205416.

(11) Guo, G. Y.; Lin, J. C. Second-harmonic generation and linear electro-optical coefficients of BN nanotubes. *Phys. Rev. B* **2005**, *72*, 075416;

(12) Wang, C.-Y.; Guo, G.-Y. Nonlinear optical properties of transition-metal dichalcogenide MX_2 (M= Mo, W; X= S, Se) monolayers and trilayers from first-principles calculations. *J. Phys. Chem. C* **2015**, *119*, 13268-13276.

(13) Hu, L.; Huang, X. R.; Wei, D. S. Layer-independent and layer-dependent nonlinear optical properties of two-dimensional GaX (X= S, Se, Te) nanosheets. *Phys. Chem. Chem. Phys.* **2017**, *19*, 11131-11141.

(14) Wang, H.; Qian, X.; Giant optical second harmonic generation in two-dimensional multiferroics. *Nano Lett.* **2017**, *17*, 5027-5034.

(15) Panday, S. R.; Fregoso, B. M. Strong second harmonic generation in two-dimensional ferroelectric IV-monochalcogenides. *J. Phys.: Condens. Matter* **2017**, *29*, 43LT01;

(16) Yang, G. Y.; Wu, K. C. Designing Two-Dimensional KBBF Family Second-Harmonic Generation Monolayers. *J. Phys. Chem. C* **2018**, *122*, 7992-7996.

(17) Guo, Y. G.; Zhu, H. Q.; Wang, Q. Large Second Harmonic Generation in Elemental α-Sb and α-Bi Monolayers. *J. Phys. Chem. C* **2020**, *124*, 5506-5513.

(18) Wu, Q.; Zhang, X.-C. Ultrafast electro-optic field sensors. *Appl. Phys. Lett.* **1996**, *68*, 1604-1606.

(19) Qiao, J. S.; Pan, Y. H.; Yang, F.; Wang, C.; Chai, Y.; Ji, W. Few-layer Tellurium: one-dimensional-like layered elementary semiconductor with striking physical properties.k *Sci. Bull.* **2018**, *63*, 159 -168.

(20) Li, I. L.; Zhai, J. P.; Launois, P.; Ruan, S. C.; Tang, Z. K. Geometry, Phase Stability, and Electronic Properties of Isolated Selenium Chains Incorporated in a Nanoporous Matrix. *J. AM. CHEM. SOC.* **2005**, *127*, 16111-16119.

(21) Churchill, H. O. H.; Salamo, G. J.; Yu, S.-Q.; Hironaka, T.; Hu, X.; Stacy, J.; Shih, I. Toward Single Atom Chains with Exfoliated Tellurium. *Nanoscale Res. Lett.* **2017**, *12*, 488.

(22) Olechna, D. J.; Knox, R. S. Energy-Band Structure of Selenium Chains. *Phys. Rev.* **1965**, *140*, A986-A993.

(23) Springborg, M.; Jones, R. O. Sulfur and selenium helices: Structure and electronic properties. *J. Chem. Phys.* **1988**, *88*, 2652-2658.

(24) Ghosh, P.; Kahaly, M. U.; Waghmare, U. V. Atomic and electronic structures, elastic properties, and optical conductivity of bulk Te and Te nanowires: A first-principles study. *Phys. Rev. B* **2007**, *75*, 245437.

(25) Kahaly, M. U.; Ghosh, P., Narasimhan, S.; Waghmare, U. V. Size dependence of structural, electronic, elastic, and optical properties of selenium nanowires: A first-principles study. *J. Chem. Phys.* **2008**, *128*, 044718.

(26) Tuttle, B.; Alhassan, S.; Pantelides, S. Computational Predictions for Single Chain Chalcogenide-Based One-Dimensional Materials. *Nanomaterials (Basel)* **2017**, *7*, 115.

(27) Andharia, E.; Kaloni, T. P.; Salamo, G. J.; Yu, S.-Q.; Churchill, H. O. H.; Barraza-Lopez, S. Exfoliation energy, quasiparticle band structure, and excitonic properties of selenium and tellurium atomic chains. *Phys. Rev. B* **2018**, *98*, 035420.

(28) Pan, Y. Y.; Gao, S. Y.; Yang, L.; Lu, J. Dependence of excited-state properties of tellurium on dimensionality: From bulk to two dimensions to one dimensions. *Phys. Rev. B* **2018**, *98*, 085135.

(29) Xiao, D.; Liu, G.-B.; Feng, W. X.; Xu, X. D.; Yao, W. Coupled Spin and Valley Physics in Monolayers of MoS2 and Other Group-VI Dichalcogenides. *Phys. Rev. Lett.* **2012**, *108*, 196802.

(30) Blöchl,P. E. Projector augmented-wave method. *Phys. Rev. B* **1994**, *50*, 17953-17979.

(31) Kresse, G.; Furthmüller, J. Efficient iterative schemes for ab initio total-energy calculations using a plane-wave basis set. *Phys. Rev. B* **1996**, *54*, 11169-11186.

(32) Kresse, G.; Furthmüller, J. Efficiency of ab-initio total energy calculations for metals and semiconductors using a plane-wave basis set. *Comput. Mater. Sci.* **1996**, *6*, 15-50.

(33) Perdew, J. P.; Burke, K.; Ernzerhof, M. Generalized Gradient Approximation Made Simple. *Phys. Rev. Lett.* **1996**, *77*, 3865-3868.

(34) Guo, G. Y.; Lin, J. C. Systematic ab initio study of the optical properties of BN nanotubes. *Phys. Rev. B* **2005**, *71*, 165402.

(35) Sipe, J. E.; Shkrebtii, A. I. Second-order optical response in semiconductors. *Phys. Rev. B* **2000**, *61*, 5337-5352.

(36) Hsueh, H. C.; Guo, G. Y.; Louie, S. G. Excitonic effects in the optical properties of a SiC sheet and nanotubes. *Phys. Rev. B* **2011**, *84*, 085404.

(37) Qiu, D. Y.; da Jornada, F. H.; Louie, S. G. Optical Spectrum of MoS_2: Many-Body Effects and Diversity of Exciton States. *Phys. Rev. Lett.* **2013**, *111*, 216805.

(38) Grüning M.; Attaccalite, C. Second harmonic generation in h-BN and MoS_2 monolayers: Role of electron-hole interaction. *Phys. Rev. B* **2014**, *89*, 081102.

(39) Trolle, M. L.; Seifert, G.; Pedersen, T. G. Theory of excitonic second-harmonic generation in monolayer MoS_2. *Phys. Rev. B* **2014**, *89*, 235410.

(40) Heyd, J.; Scuseria, G. E.; Ernzerhof, M. Hybrid functionals based on a screened Coulomb potential. *J. Chem. Phys.* **2003**, *118*, 8207-8215.

(41) Young, S. M.; Rappe, A. M. First Principles Calculation of the Shift Current Photovoltaic Effect in Ferroelectrics. *Phys. Rev. Lett.* **2012**, *109*, 116601.

(42) Reshaka, A. H. First-principle calculations of the linear and nonlinear optical response for GaX (X = As, Sb, P). *Eur. Phys. J. B* **2005**, *47*, 503-508.

(43) Kong, F. J.; Liu, Y. L.; Hu, Y. F.; Hou, H. J.; Hu, F. Density functional theory calculations insight to the effect of anion on the nonlinear optical properties of $LiInX_2$ (X = S, Se). *J. Mol. Model.* **2014**, *20*, 2528.

(44) Hu, L.; Wei, D. S. Second-order nonlinear optical properties of bulk GeC polytypes, g-GeC and corresponding nanotubes: first-principles calculations. *Phys.Chem.Chem.Phys.* **2017**, *19*, 2235-2244.

(45) Hu, L.; Huang, X. R. Peculiar electronic, strong in-plane and out-of plane second harmonic generation and piezoelectric properties of atom-thick α-M_2X_3 (M = Ga, In; X = S, Se): role of spontaneous electric dipole orientations. *RSC Adv.* **2017**, *7*, 55034-55043.

(46) Jiang, S. J.; Yin, H. B.; Li, J.Y.; Liu, L.; Shi, X. B.; Yan, Y. L.; Liu, C.; Zheng, G.-P.; Liu, P.-F. Multidirectional Intrinsic Piezoelectricity of 2D Metal Chalcogen-Diphosphate ABP_2X_6 Monolayers. *Phys. Status Solidi RRL* **2020**, *14*, 2000321.

(47) Ouahrani, T.; Reshak, A. H.; Khenata, R.; Baltache, H.; Amrani, B.; Bouhemadou, A. Structural, electronic, linear, and nonlinear optical properties of $ZnCdTe_2$ chalcopyrite. *Phys. Status Solidi B* **2011**, *248*, 712-718.

(48) Ma, Z. J.; Hu, J. Y.; Sa, R. J.; Li, Q. H.; Zhang, Y. F.; Wu, K. C. Screening novel candidates for mid-IR nonlinear optical materials from I_3-V-VI_4 compounds. *J. Mater. Chem. C* **2017**, *5*, 1963-1972.

(49) Lin, Y.-J.; Liu, B.-W.; Ye, R.; Jiang, X.-M.; Yang, L.-Q.; Zeng, H.-Y.; Guo, G.-C. $SrCdSnQ_4$ (Q = S and Se): infrared nonlinear optical chalcogenides with mixed NLO-active and synergetic distorted motifs. *J. Mater. Chem. C* **2019**, *10*, 1039.

(50) Jiang, X. X.; Zhao, S. G.; Lin, Z. S.; Luo, J. H.; Bristowe, P. D.; Guan, X. G.; Chen, C. T.; The role of dipole moment in determining the nonlinear optical behavior of materials: ab initio studies on quaternary molybdenum tellurite crystals. *J. Mater. Chem. C* **2014**, *2*, 530-537.

(51) Cammarata, A.; Zhang, W. G.; Halasyamani, P. S.; Rondinelli, J. M. Microscopic origins of optical second harmonic generation in noncentrosymmetric-nonpolar materials. *Chem. Mater.* **2014**, *26*, 5773-5781.

(52) Ingers, J.; Maschke, K.; Proennecke, S. Optical-transition-matrix elements between

localized electronic states in disordered one-dimensional systems. *Phys. Rev. B* **1988**, *37*, 6105-6112.

(53) Song, J.-H.; Freeman, A. J.; Bera, T. K.; Chung, I.; Kanatzidis, M. G. First-principles prediction of an enhanced optical second-harmonic susceptibility of low-dimensional alkali-metal chalcogenides. *Phys. Rev. B* **2009**, *79*, 245203.

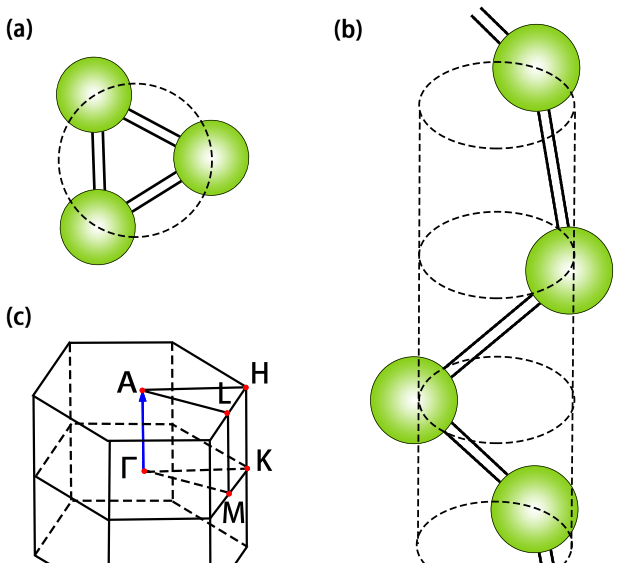


Figure 1: (a) Top and (and tellurium as well as (c) the associated $\vec{k}$ path ated by blue arrow.

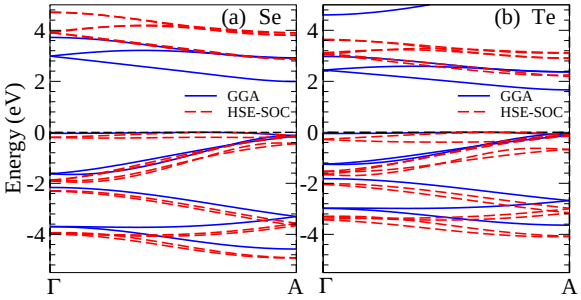


Figure 2: Band structures of (a) selenium and (b) tellurium chains from the GGA (blue solid lines) calculations and HSE (red dashed lines) calculations with the SOC included. Both materials possess indirect band gaps. The top of the valence bands is at 0 eV.

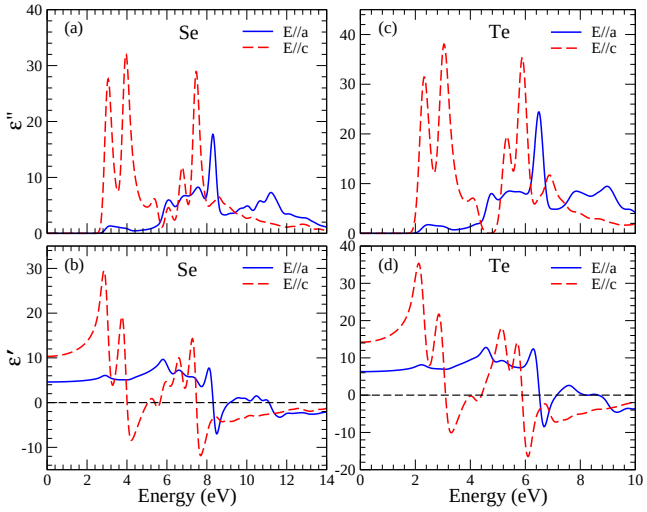


Figure 3: Calculated imaginary $[\varepsilon''(\omega)]$ and real $[\varepsilon'(\omega)]$ part of the dielectric function for (a) and (b) selenium chain as well as (c) and (d) tellurium chain for light polarization perpendicular (E‖a) and parallel (E‖c) to the c axis.

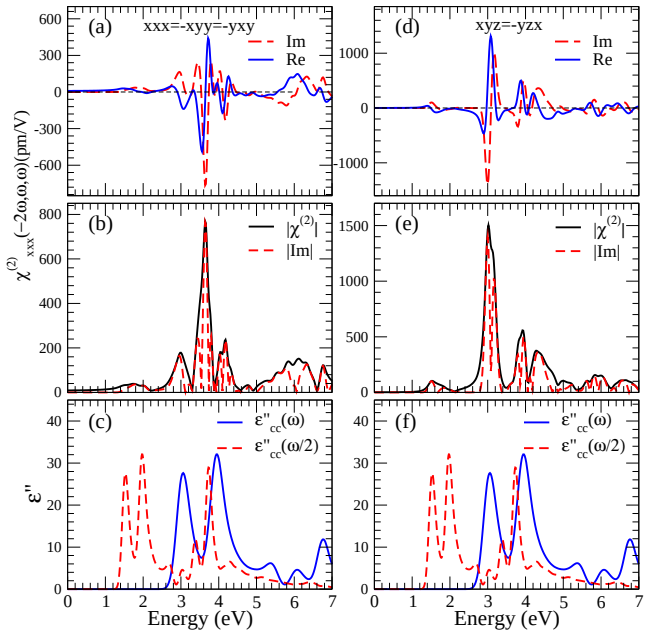


Figure 4: (a) and (d) Real and imaginary parts of the second-order susceptibility for $\chi^{(2)}_{xxx}$ and $\chi^{(2)}_{xyz}$ in selenium chain, respectively. (b) and (e) Absolute value of the second-order susceptibility for $\chi^{(2)}_{xxx}$ and $\chi^{(2)}_{xyz}$ in selenium chain, respectively. (c) and (f) Imaginary part of the dielectric function for light polarization parallel to the c axis.

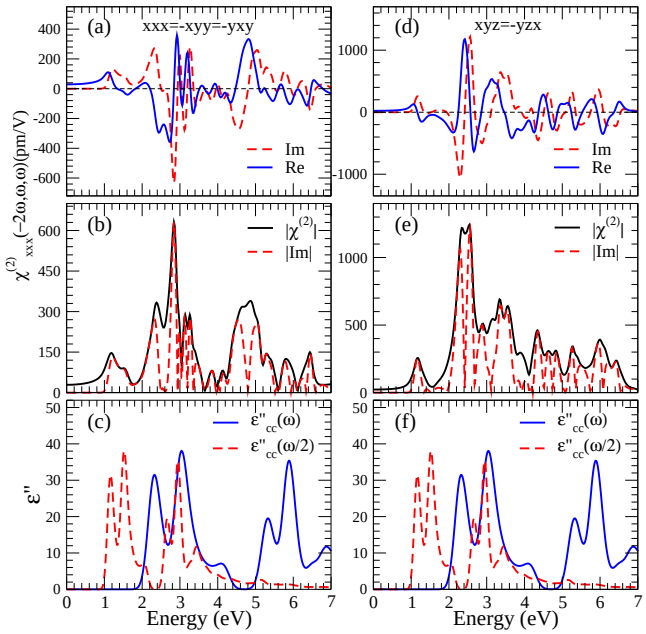


Figure 5: (a) and (d) Real and imaginary parts of the second-order susceptibility for $\chi^{(2)}_{xxx}$ and $\chi^{(2)}_{xyz}$ in tellurium chain, respectively. (b) and (e) Absolute value of the second-order susceptibility for $\chi^{(2)}_{xxx}$ and $\chi^{(2)}_{xyz}$ in tellurium chain, respectively. (c) and (f) Imaginary part of the dielectric function for light polarization parallel to the c axis.

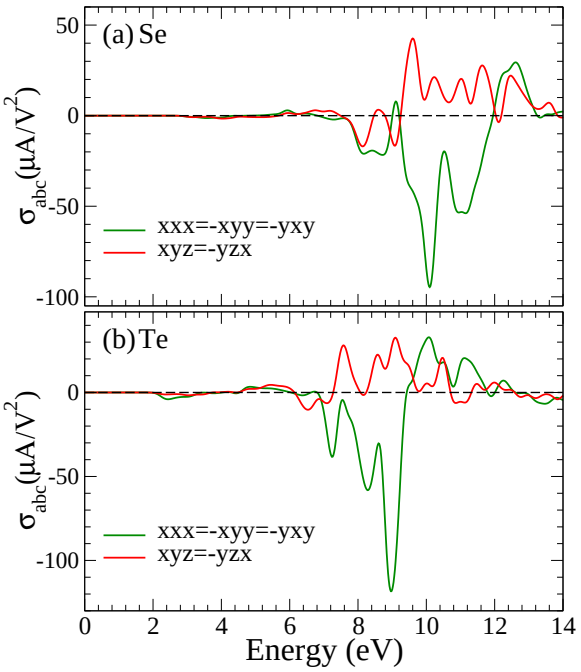


Figure 6: The shift current response (σ) versus the photon energy for one-dimensional (a) selenium and (b) tellurium.

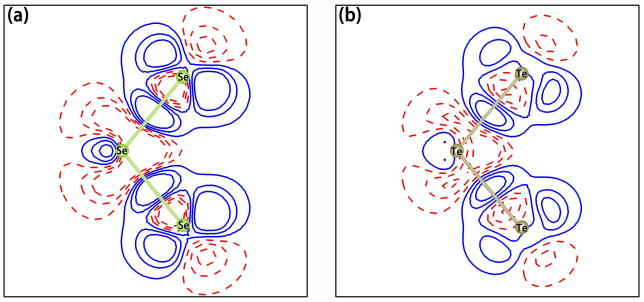


Figure 7: The contour plots of the deformation charge densities for one-dimensional (a) selenium and (b) tellurium. The contour interval is 0.02 e/Å^3. The electron accumulation is depicted by positive contours (blue solid lines), while the electron depletion is represented by negative contours (red dashed lines)